Engineering Failure Analysis 177 (2025) 109675

Contents lists available at ScienceDirect

Engineering Failure Analysis

journal homepage: www.elsevier.com/locate/engfailanal

Innovative non-destructive thermographic evaluation of mechanical properties in dissimilar aluminium probeless friction stir spot welded (P-FSSW) joints

G. Dell'Avvocato [a,*], M. Rashkovets [b,c], E. Mancini [a], N. Contuzzi [b], G. Casalino [b], D. Palumbo [b], U. Galietti [b]

[a] Department of Industrial and Information Engineering and Economics (DIIIE), University of L'Aquila, L'Aquila, Italy
[b] Department of Mechanics, Mathematics and Management (DMMM), Polytechnic University of Bari, Bari, Italy
[c] World-class research Center "Advanced Digital Technologies", State Marine Technical University, St. Petersburg, Russian Federation

ARTICLE INFO

Keywords:
Laser thermographyl
Probeless Friction Stir Spot Welding (P-FSSW)
NDT
Mechanical properties
Aluminium alloys welding
Welding quality assessment

ABSTRACT

This study introduces a novel non-destructive methodology based on step-heating laser thermography technique to evaluate the mechanical strength of dissimilar aluminium joints produced through probeless friction stir spot welding (P-FSSW). The proposed approach enables the quantitative analysis of the thermo-mechanically stirred region, distinguishing two different morphologies (ductile and mixed) correlated with the joint's ultimate mechanical strength. Eleven welded joints were analysed by using two of them used for calibration through thermographic tests, Chisel and scanning electron microscopy (SEM) analyses. At the same time, nine underwent tensile-shear tests were carried out to correlate thermographic parameters (A_1, A_2) with maximum force (F_{max}).

Statistical analysis revealed that the ductile area (A_2) is the most significant parameter, exhibiting a robust correlation with Fmax ($r = 0.81$). A simplified regression model based on A_2 demonstrated high reliability (adjusted $R^2 = 0.60$). This methodology provides a significant advancement in non-destructive quality control for P-FSSW joints, paving the way for its integration into industrial applications. The developed procedure offers a reliable, contactless, and scalable solution for real-time industrial inspection of P-FSSW joints, representing a significant alternative to conventional destructive testing methods.

1. Introduction

To address the ongoing climate crisis, significant efforts are required across all sectors, particularly in transportation, where challenges such as fuel economy, cost reduction, recyclability, aend emissions mitigation are critical. In this context, research focuses on alternative fuels—e.g., in aviation [1,2] —and fuel cell adoption in naval [3] and automotive industries [4], the latter being a major contributor to global emissions.

One of the most effective strategies to meet these goals is vehicle lightweighting, initially developed for military and sport applications [5,6] and now widely adopted in civilian transportation. Promising solutions include composite materials, metamaterials

* Corresponding author.
E-mail address: giuseppe.dellavvocato@univaq.it (G. Dell'Avvocato).

https://doi.org/10.1016/j.engfailanal.2025.109675
Received 10 March 2025; Received in revised form 30 April 2025; Accepted 1 May 2025
Available online 8 May 2025

[7], high-strength steels (HSSs) [8], and lightweight alloys [6,9]. Among these, aluminium alloys are particularly attractive due to their excellent mechanical properties, in some cases comparable to steels.

The widespread use of aluminium in transportation demands new joining and manufacturing solutions [9,10]. Traditional methods like riveting or bolting provide reliable joints but increase weight and costs. Adhesive or welded joints, by avoiding drilling operations, reduce weight and improve production efficiency.

However, welding aluminium remains challenging due to its high thermal conductivity [11], which limits the applicability of many fusion-based processes. As a result, solid-state techniques such as friction welding, ultrasonic welding, and diffusion bonding [12–16] have gained relevance. Among them, friction stir welding (FSW) is especially promising, offering high mechanical strength and compatibility with various materials [13,17–20]. For these reasons, FSW has found widespread use in the automotive, naval, and aeronautical sectors [21].

One of the recent variations of FSW is probeless (or pinless) friction stir spot welding (P-FSSW) [13,17–19,22,23]. This technique uses a pinless tool to effectively overcome the keyhole defect commonly observed at the centre of spot welds produced by conventional FSSW [17]. The friction generated by the pressure and rotation of the tool on the surface of two overlapping thin sheets produces heat, raising the material's temperature to a softening point. This allows the rotating tool to stir joining materials, thereby forming a weld spot with a nominal size equal to that of the tool itself [13,17–19,22,23].

A significant limitation to the widespread adoption of adhesive or welded joints lies in the lack of reliable non-destructive testing (NDT) methods to verify joint quality and mechanical strength. Evaluating the integrity of welded joints and their mechanical characterization has always been a critical aspect of mechanical design, enabling robust reliability-based design. To promote their use, whenever a new joining process is developed, a comprehensive mechanical characterization of the joints is necessary to evaluate not only the process parameters that ensure the best mechanical properties but also those parameters of features directly related to the mechanical strength of the joints. For example, in the case of spot welds in general, such as resistance spot welding (RSW) or resistance projection welding (RPW), the area of the fused region is indicative of the final joint's mechanical strength [24–30].

Once the characteristics indicative of the mechanical strength of the welded joints have been identified, these are used to verify the joint's quality after production, ensuring the designed mechanical properties are achieved. Generally, there are two possible approaches to accomplish this goal: destructive tests, such as the Chisel test or metallography for quantifying the fused region, or non-destructive tests capable of quantifying the fused region or detecting internal defects. In the case of destructive tests, a major limitation is the need to perform tests on a sample basis, which requires sacrificing material and processing for testing without ensuring the quality of 100 % of production. On the other hand, non-destructive tests (NDT) do not alter or influence the joint under examination and have the advantage of being applicable to 100 % of production. However, they require a robust initial calibration phase, as they are comparative methods.

Therefore, non-destructive testing is essential for assessing the integrity of welded joints without altering their properties, which is why it is widely used in industry. For welded joints, both volumetric and surface tests are performed using techniques such as ultrasonic testing (UT) or X-rays [31–33] and liquid penetrants (PT) or magnetic particle (MT) for surface inspections. Each of these tests, however, has its limitations, which is why a volumetric test is often combined with a surface test to achieve a complete evaluation. One of the leading technical limitations of UT is the minimum inspectable thickness, as is the case with X-rays. Additionally, the testing and analysis times for these two techniques are time consuming, making them less attractive for high-volume manufacturing.

Several studies have been conducted to address these limitations. For example, Liu et al. [32], developed an inspection system based on ultrasonic probes integrated into electrodes to monitor the nugget diameter in real-time during spot welding, enabling process monitoring. The system generates B-scan images that allow observation of the nugget's growth and solidification, improving in-line inspection efficiency. However, the method has limitations, including the need for accurate calibration due to its high sensitivity to changes in the speed of sound in the molten metal, especially for very thin joints.

Ghafarallahi et al. [34], proposed an approach based on numerical simulations and artificial neural networks (ANNs) to analyse ultrasonic signals. This method allows for a highly accurate prediction of nugget diameter in three-layer welded joints. However, one of the main limitations of this technique is the need for a large number of samples to adequately train the neural network, making the initial implementation phase labour-intensive and time-consuming. Additionally, it requires the development of a multiphysics model of the production process.

Sun et al. [27], demonstrated the effectiveness of ultrasonic C-scan for analysing the quality of resistance-welded joints, highlighting a significant correlation between ultrasonic signals and internal defects, such as nugget size. However, this method requires long processing times to comprehensively analyse the acquired data, as the analysis of C-scan images involves detailed and often manual processing, making it poorly suited for in-line industrial applications and automation.

Chertov et al. [35], introduced an acoustic model to simulate the propagation of ultrasonic waves in spot-welded joints and estimate the nugget diameter based on the analysis of reflected and transmitted waves. While innovative, this work has three main limitations: it relies heavily on simulated data, requires significant calibration and experimental validation to ensure reliable results, struggles with low-thickness joints due to wave attenuation and dispersion, and is overly sensitive to small variations in transducer positioning or acoustic parameters, limiting its practical application in industrial environments.

To overcome these limitations, thermographic non-destructive testing (TNDT) can be a viable alternative. Active thermography techniques offer several advantages over UT techniques, including full-field inspections, no need for contact with the component's surface, very short inspection times, and suitability for implementation in automated in-line controls. Because of these advantages, thermographic techniques have been confirmed as very versatile methods for defect detection in different materials [36–38] and material characterization, as well as mechanical [39,40] and thermal [41–46].

The scientific community's interest in this direction remains very high. For example, Sriyubol et al. [47], proposed using pulsed

thermography to maximize cross-correlation and identify brazed joint defects. This technique showed greater sensitivity to noise compared to traditional methods, with improved capability to predict defect dimensions. However, the approach is limited by the mathematical complexity of the inverse problem, making it highly dependent on the collected data's quality and precise experimental configuration.

Myrach et al. [48], implemented a calibration method for active thermography using X-ray computed tomography to validate the measurements of nugget diameter in resistance-welded joints. This method enabled accurate, non-contact joint evaluations but was constrained by the need for a significant initial calibration effort, making it less practical for high-production industrial applications.

In two separate studies, Santoro et al. [49,50], explored the use of active thermography to estimate the quality of resistance-welded joints. The first study used the methodology to analyse thermally modulated signals to evaluate the nugget and corona bond dimensions [50]. In the second, they integrated a convolutional neural network (CNN) to analyse thermal signal phase and amplitude gradient maps, automating the estimation of joint quality. These approaches are promising, as they are easily automatable and capable of correlating thermal characteristics with the mechanical properties of joints. However, both studies present certain limitations, including the need for large datasets to train the neural network, the requirement for precise system calibration, and the technique's sensitivity to surface conditions of the joint, which necessitates careful preparation to achieve reliable results.

Palumbo and Galietti [51], explored the application of infrared thermography to characterize fatigue in steel-welded joints, showing that variations in the phase of the thermoelastic signal could be correlated with structural damage. Although the method is promising, it is negatively influenced by the high thermal conductivity of materials like aluminium alloys, which are the focus of the present work. Extensive analysis is required to avoid errors in the results.

Dell'Avvocato and Palumbo [25], proposed a non-destructive procedure based on flash thermography for quantitatively evaluating the fused region in thin joints obtained via RPW with rectangular geometry. This procedure allowed the estimation of the joint's mechanical strength from the geometry detected by thermography. One limitation of this procedure, namely the need to cover the surface to enhance absorption, was overcome by the same authors using a high-energy–density source, such as a laser source [52]. This enabled the development of a procedure suitable for "as-is" surfaces, resulting in a quantitative evaluation of the fused region geometry comparable to that obtained through advanced UT techniques. However, a significant limitation of the proposed procedure remains the need for high energy densities and, consequently, a costly setup that is more challenging in terms of operator safety compared to flash thermography.

All the aforementioned works, undoubtedly represent significant advancements and confirm the suitability of thermographic techniques for evaluating thin welded joints. However, they mainly focus on welds produced by traditional fusion methods such as RSW or brazing. In the case of solid-state welding, several significant studies in the literature have investigated joints obtained through FSW using thermographic techniques. Some of these studies focus on process monitoring [53,54], while others use offline non-destructive testing to evaluate the joint's mechanical strength and detect internal defects [55]. Moreover, regarding novel joining techniques like P-FSSW—the method used to produce the joints examined in the present work—no existing non-destructive procedures based on thermographic techniques evaluate the possibility of characterizing this type of joint in a fully non-destructive manner.

For this reason, some of the authors of the present work previously conducted a preliminary study in which a quantitative evaluation procedure for the joining region in P-FSSW joints of thin aluminium plates was proposed [56]. The cited preliminary study, which represented the first step in a broader research effort, compared thermographic results with those obtained through UT.

Given the limitations of traditional NDT techniques for thin joints, the absence of quantitative non-destructive procedures for P-FSSW joints, and the lack of specific studies on NDT techniques capable of mechanically characterizing these joints, this study positions itself precisely within this context. Specifically, this study aims to propose a laser thermography-based control procedure to estimate the mechanical properties of dissimilar aluminium P-FSSW joints in a fully non-destructive way. Additionally, using long heating times and managing non-uniform heating through laser spots aim to propose a simplified experimental setup and testing procedure compared to the impulsive excitation methods cited in the literature.

To achieve this goal, various P-FSSW specimens were produced and tested by laser thermography. Subsequently, some of the specimens were subjected to mechanical tests such as the Chisel test and fracture surface analysis, the results of which were used to calibrate the proposed analysis procedure. The thermographic results from the remaining specimens were analysed using the same procedure before undergoing tensile-shear mechanical tests. Statistical tools were used to evaluate the correlation between thermographic results and experimentally obtained mechanical strength, allowing for the identification of parameters that most significantly influence mechanical strength and proposing a model capable of estimating joint strength based on thermographic test results.

For the first time, an NDT procedure based on laser thermography has been developed for P-FSSW aluminium dissimilar joint. An additional innovative aspect lies in the use of active thermography, not only to detect and quantify the welded region in a P-FSSW joint but also to distinguish between two different morphologies of the welded region by studying their correlation with the final mechanical strength.

2. Materials and methods

2.1. Theory

To analyse the temperature evolution over time during step heating, it is necessary to describe the surface temperature behaviour following heating with a laser source. In the present case, the heating process via the laser source can be modelled as a spatially Gaussian heat distribution applied for a finite duration τ, incorporating the Heaviside function $\chi(t)$ over time. In this scenario, considering the convolution integral over the interval $[t_0 - \tau/2, t_0 + \tau/2]$ to represent step heating over time $T(x, y, 0, t) =$

$$\int_{t_0-\tau/2}^{t_0+\tau/2} \frac{2Q_0}{\pi} \frac{e^{-\frac{x^2+y^2}{\sigma_t^2}}}{\sigma_t^2} \left[\frac{1}{\rho C L} \left(1 + 2\sum_{n=1}^{\infty} e^{-\frac{n^2\pi^2\alpha_n t}{L^2}} \right) \right] \bullet \chi(t) dt_\tau (1).$$

where Q is the absorbed heat, σ_t is the standard deviation of the Gaussian distribution, ρ the density, C the specific heat, L the thickness of the plate, α_n is the thermal diffusivity in the thickness direction. This analysis assumes adiabatic heat exchange, finite body dimensions and homogeneous material. This equation effectively describes the transient thermal response of the material subjected to step heat, providing a foundation for further thermographic analysis.

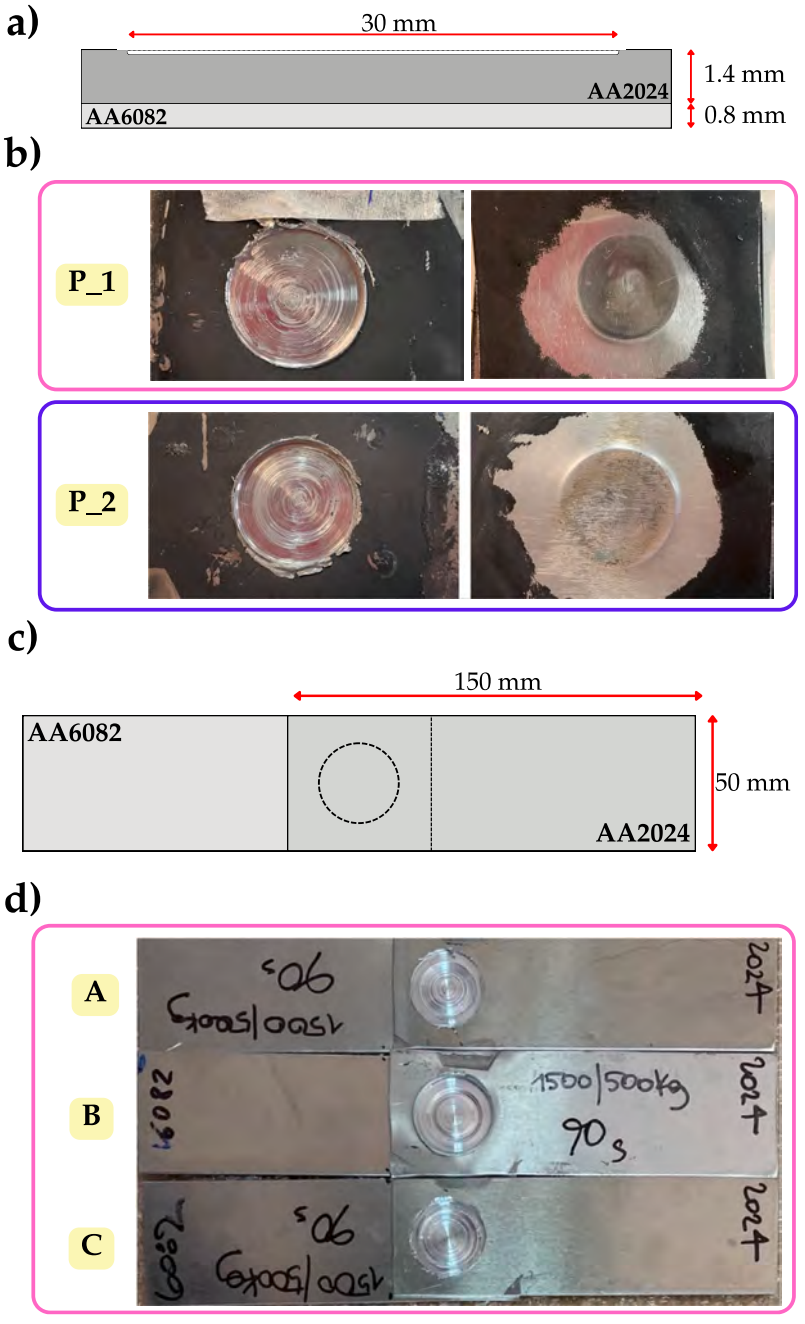

Fig. 1. (a) Scheme of the geometry of joints P_1 and P_2. (b) Real pictures of specimens P_1 and P_2 from front and rear side. (c) Scheme of the geometry of specimens produced for tensile test. (d) Real pictures of three specimens analysed in the research work.

2.2. Specimens

The welds under investigation, as previously mentioned, were obtained through the P-FSSW process. This technique was employed to join two aluminium sheets of different thicknesses: 0.8 mm (AA2024-T3) and 1.4 mm (AA6082-T6). To produce the lap-joint, a tool with a nominal diameter of 30 mm was positioned in contact with the surface of the thicker AA6082-T6 plate, applying a force of 4.9 kN for 90 s. Two distinct groups of specimens were produced to evaluate the capability of thermography in assessing the quality of these welded joints.

First, two specimens, P_1 and P_2, were joined using two different rotational speeds of 2500 rpm and 2000 rpm, respectively. The geometry is illustrated in in Fig. 1 a-b.

Based on a preliminary numerical and exeperimental investigations [17], these parameters were selected to ensure that the two specimens exhibited significantly distinct characteristics. The second group of specimens was manufactured as lap joints to enable subsequent mechanical tensile-shear testing. This second group of specimens (Fig. 1 c-d) was produced using three different rotational speeds (1500 rpm, 2000 rpm, and 2500 rpm), as described in a previous work [23] with three replicates for each speed, resulting in nine specimens, as summarized in Table 1.

Welding force and dwell time were kept constant throughout the experimental campaign, as previous investigations [17] demonstrated their critical influence on material softening and material flow behavior during the P-FSSW process. Regarding tool plunge depth, the welding machine operated in force-control mode after an initial plunge of 0.1 mm into the first plate; consequently, the plunge depth varied automatically to maintain the preset welding force and was not treated as an independent process variable. Therefore, the present study focuses specifically on the influence of rotational speed while keeping the other parameters constant and optimized.

As shown in Fig. 1 a-c, which present the actual images of the analysed specimens, the tool leaves a pronounced imprint on the welded surface, characterized by substantial surface inhomogeneity, particularly in roughness. The opposite side, corresponding to the thinner AA2024-T3 plate, exhibits a more uniform appearance but with noticeable variations in emissivity and slight plastic deformations caused by the welding process. To mitigate the influence of non-uniform surface emissivity, the joints were coated with a thin, uniform layer of high-emissivity black paint, approximately 0.98, to uniform the emissivity across the entire surface of the specimen.

2.3. Experimental setup

As described above, one surface of each specimen was coated with a thin layer of high-emissivity black paint to standardize emissivity. Each specimen was inspected from painted surface side using a reflection setup, as shown in Fig. 2. This surface, corresponding to the weld joint, was heated using an Ytterbium pulsed fibre laser source (YLP-V2 mJ series) with a wavelength of approximately 920 nm, a nominal power of 50 W, and a circular laser spot with a Gaussian distribution and a diameter of about D = 45 mm. This ensured complete heating of the welded region, which has a D = 30 mm nominally. Due to the low surface energy density available and considering the high thermal conductivity of the materials, the step heating technique was adopted, with a heating duration of approximately 1 s.

The laser source was tilted at approximately 5° relative to the inspected surface to allow for a frontal positioning of the thermal camera. The heating phase (~1 s) and the cooling phase (~2 s) were recorded for a total duration of ~ 3 s using a FLIR LW thermal camera equipped with a cooled sensor. The camera operated at an acquisition frequency of 2500 Hz, achieved by reducing the window size to 196 × 224 pixels^2, with a calibration range of −20 °C to 150 °C and a spatial resolution of 0.226 mm/pixel. As depicted in Fig. 2, the inspection area was suspended for both specimen geometries to avoid contact with metallic supports in regions close to the inspected zones.

Specimens P1 and P2 were subjected to chisel tests, followed by failure analysis using scanning electron microscopy (SEM, Tescan Mira3) with secondary electron (SE) mode.

A servo-hydraulic testing machine (MTS Model 370 Load Frame) was employed for the mechanical tests on the second group of specimens. This machine features a rigid double-column structure and a load cell with a capacity of ± 100 kN while, the tests were carried out controlling the displacement at a 1 mm/min rate. As shown in Fig. 3, the second group of specimens was tested by inserting spacers cut directly from the main plates of the analysed specimens between the welded plates and the grips of the load machine. This arrangement minimized load eccentricity.

The tests applied a tensile-shear load at the two ends of the joint as reported in Fig. 3**d**. However, given the geometry, the load state in the joint cannot be considered uniaxial. Therefore, the maximum force recorded during the tests was used as the metric for evaluating the mechanical strength of the joint.

Table 1
Description of process parameters for investigated specimens.

Specimen	Rotational speed (rpm)	Force (kN)	Time (s)	Replications
A	1500	4.9	90	3
B	2000	4.9	90	3
C	2500	4.9	90	3

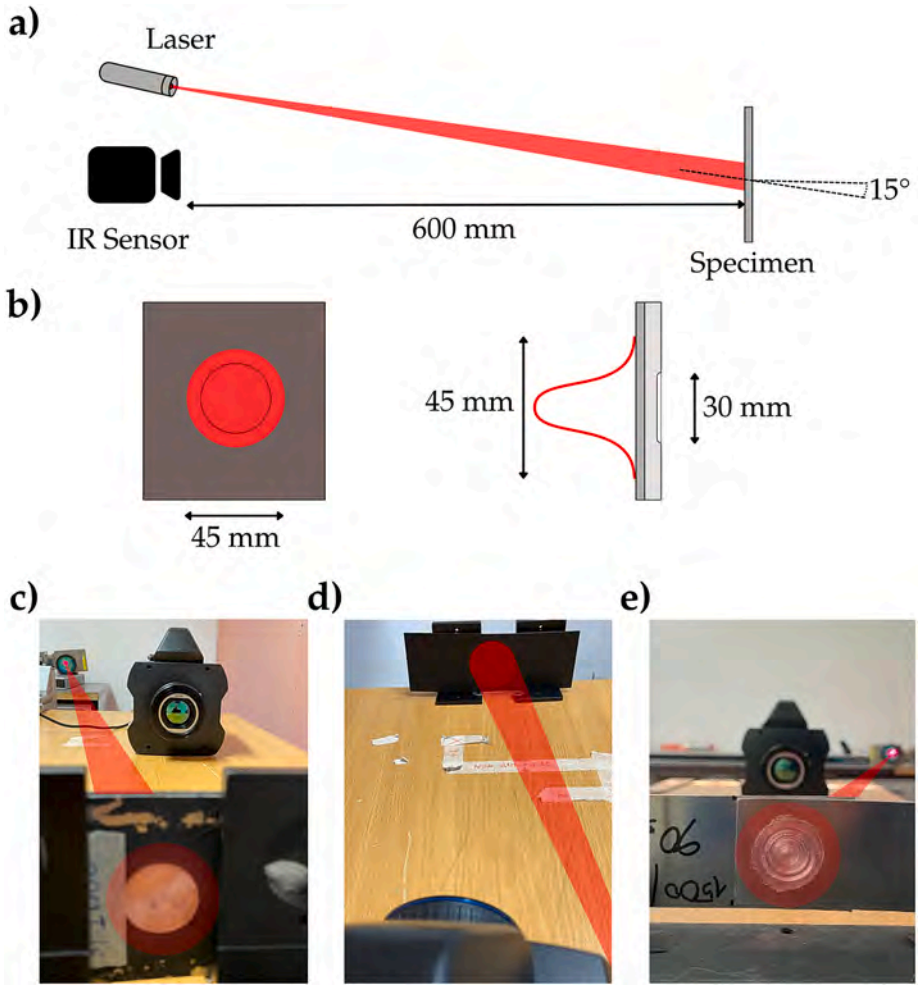

Fig. 2. (a) Scheme of the set-up adopted for the thermographic tests. (b) Scheme of the heating distribution of laser on the inspected surface and the relative position of welded joint. c-d) Real picture of the thermographic setup adopted for the first group of specimens and e) for the second group.

2.4. Methods

In the introduction, it was previously highlighted that spot welds can be evaluated in multiple ways. One approach is to assess their final mechanical strength through mechanical testing, while another is to quantify the welded area of the spot weld, which is typically correlated with the joint's final mechanical strength. The latter approach requires an initial study to verify this correlation between area and mechanical strength, commonly exploited in NDT methodologies.

Since P-FSSW is an innovative welding process, it is first necessary to establish whether such a correlation exists and, if so, to determine its nature. Subsequently, the feasibility of developing a non-destructive procedure based on laser thermography must be investigated. This procedure would measure the welded area and interpret the results to estimate the joint's final strength.

To achieve this, as previously mentioned, specimens were produced with two different final geometries but using the same machine and process, varying only the rotational speed. The sole purpose of differing geometries was that P_1 and P_2 were subjected to Chisel tests and SEM analysis of the fracture surface. In contrast, the second group of specimens underwent mechanical testing to determine their maximum strength, providing a quantitative measure of their mechanical resistance.

All specimens were subjected to thermographic tests using the setup described above. Each test was repeated three times to account for measurement repeatability. Given the long heating duration employed in the "stepped" approach, conventional post-processing algorithms commonly used in pulsed thermography were not applicable [57]. These algorithms rely on impulsive, one-dimensional heating assumptions, which are invalid in this context.

The assumption of impulsive heating fails because the heating duration far exceeds the characteristic time for an impulsive thermal wave to traverse twice the thickness of the component—consequently, the heating phase overlaps with the arrival of the initial thermal reflections at the surface. Similarly, the assumption of one-dimensional heat flow is invalid due to the Gaussian distribution of heat (and temperature) across the inspected surface. Despite the large diameter of the laser spot and its high standard deviation, the

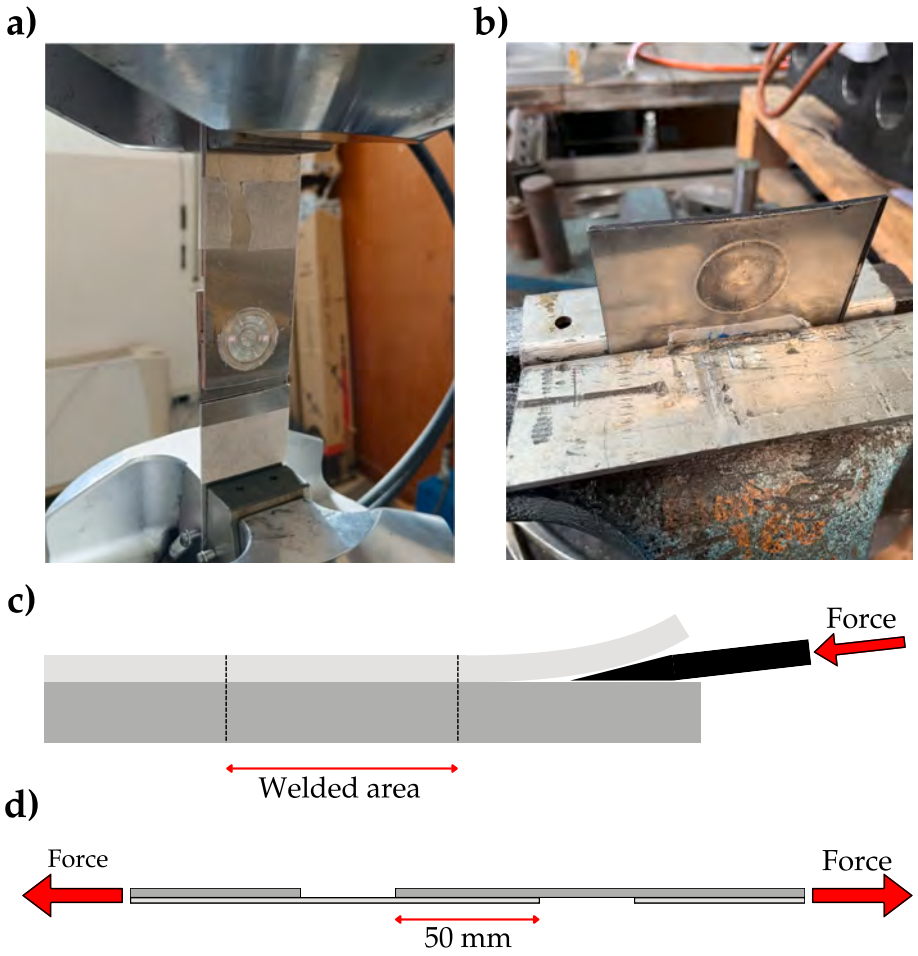

Fig. 3. (a) Experimental set-up for tensile tests. (b) Experimental set-up for Chisel tests. (c)Scheme of Chisel test. (d) Scheme of tensile-shear tests.

temperature is not uniform within the spot. It is higher at the centre and lower toward the periphery, generating radial lateral heat fluxes that preclude the validity of the one-dimensional flow assumption that are traditionally adopted for thermal NDT.

The proposed procedure addresses these challenges through a comparative approach. Following the weld tests, an additional test was performed under the same highly repeatable setup on a "reference specimen." This reference specimen consisted of two identical plates joined using adhesive tape, as shown schematically in Fig. 4 a. These plates serve as a thermal reference for plates in contact but not welded. In such cases, the thermal resistance at the interface impedes heat transfer to the rear plate, causing a more significant temperature increase on the front plate. In contrast, the interfacial thermal resistance in welded joints is lower or negligible, allowing for easier heat flow from the upper plate to the lower plate, resulting in a lower temperature on the inspected surface.

Thermal contrast is typically evaluated based on these behaviours to distinguish a welded region from an unwelded one. This is defined as the temperature difference between a welded region and an unwelded region by subtracting the average temperature value of an unwelded area from each pixel [57]. However, this approach is meaningful only for uniform heating. Given the Gaussian temperature distribution and the peripheral location of unwelded areas within the laser spot, direct subtraction of this value from each pixel would yield insignificant results due to the heating gradient across the spot. To overcome this limitation, a direct subtraction between frames was performed to eliminate the influence of the heat distribution.

In step heating tests, the final heating frame (or the first cooling frame) is often used for analysis, as documented in the literature [58,59]. This criterion was adopted for the tests in question. The following procedure was performed for each sequence: the final heating frame was subtracted from a "cold frame", obtained by averaging twenty frames recorded before heating began, resulting in a frame indicating the temperature difference caused by heating (ΔT_w) showed in Fig. 5. The exact process was applied to the reference specimen, yielding a frame (ΔT_{nw}) representing the temperature distribution if the plates were in contact without welding (Fig. 5). Subsequently, the reference frame was subtracted from each welded joint test frame ($\Delta T_c = \Delta T_{nw} - \Delta T_w$) (Fig. 5). The resulting frame highlights temperature distribution differences solely due to the presence or absence of a welded region, with an intensity proportional to the contact thermal resistance and the thermophysical property differences of the welded region.

If no welding occurs, the thermal behaviour of the joint would be similar to that of two overlapping plates, yielding minimal differences. Conversely, an adequately welded joint would exhibit significant differences from the overlapping plates. The resulting

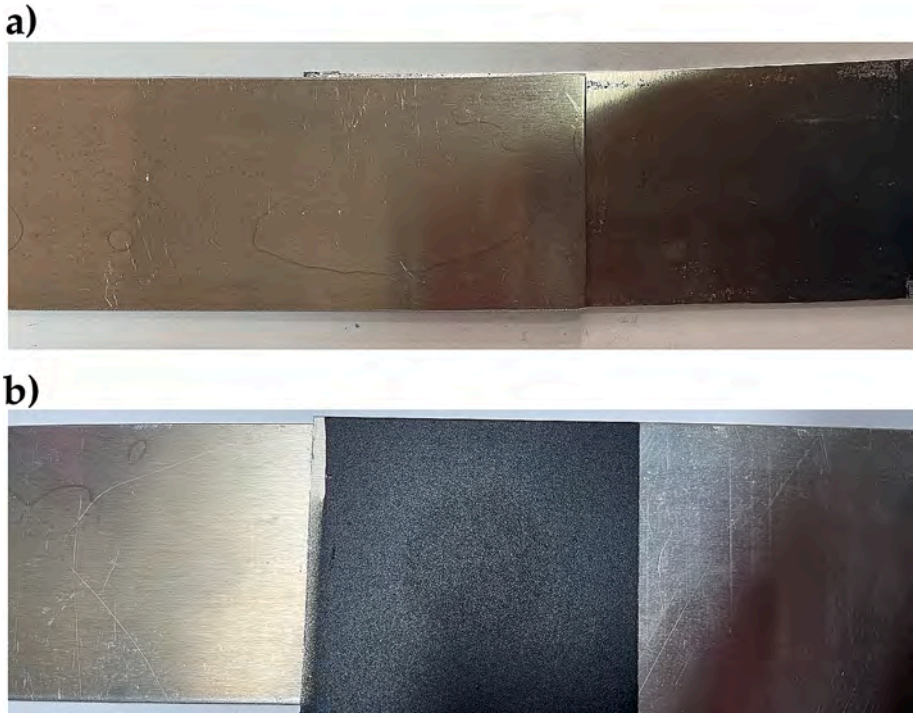

Fig. 4. (a) Two overlapped plates adopted as reference specimen for the non-welded behaviour. (b) Detail of inspected coated surface of welded specimen before the tensile-shear test.

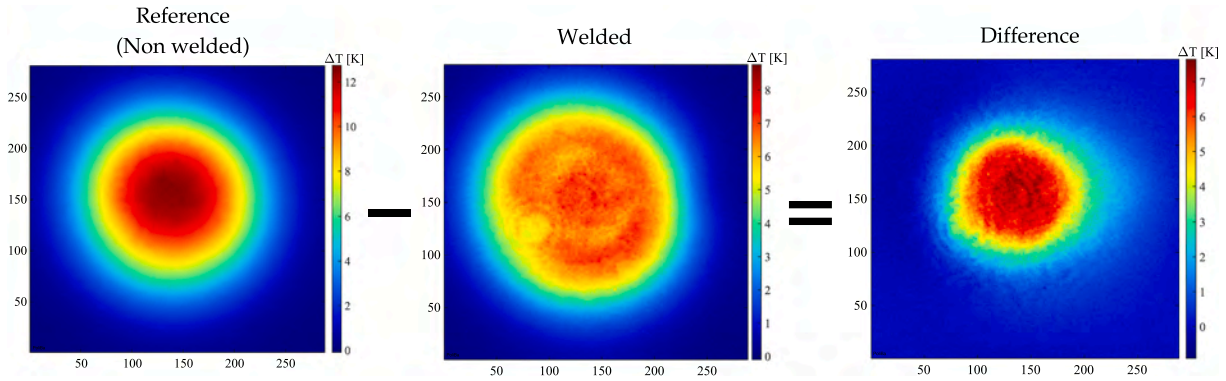

Fig. 5. Representation of the subtraction between reference thermogram and thermogram from welded area and the obtained "difference thermogram".

thermal contrast maps were then normalized to produce Normalized Thermal Contrast (NTC) maps [60]. NTC is an indicator of signal intensity relative to background noise, commonly used in the literature to establish thresholds for defect detection [25,52,60] or distinguishing welded from unwelded regions [25,52]. It is defined as:

$$NTC = \frac{\Delta T_c}{\sigma_{non-weld}} \tag{3}$$

where $\sigma_{non-weld}$ is the standard deviation of the temperature within a reference unwelded area.

Specimens P_1 and P_2 were subsequently subjected to Chisel tests and fractographic analysis to define the welded region for both specimens. Specifically, following the fracture analysis of specimen P_1, thermographic image analysis was conducted in a MATLAB environment. This process established NTC thresholds for segmenting the thermographic images, providing a calibration to define threshold values applicable to all other specimens.

The fractographic analysis of specimen P_1 revealed two distinct morphologies within the welded region which are related to the mechanical behaviour of joint. Specifically, the results displayed features of ductile failure within the outer region (Fig. 6 a) and

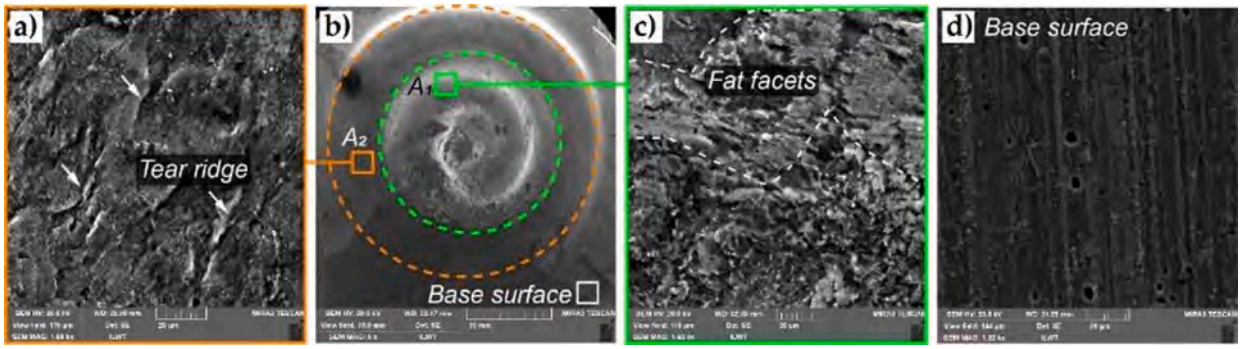

Fig. 6. SEM of specimen P_1: (a) ductile fracture of the outer region with characteristic feature of tear rides. (b) overall view of the fracture surface on the upper sheet. (c) mixed fracture of the inner region with the presence of flat facets. (d) the surface of the base metal.

ductile–brittle (mixed) behaviour along the inner region (Fig. 6 c) with the presence of flat facets (indicated by dashed lines on Fig. 6 c). These brittle features may suggest the formation of micro-cracking within the highly deformed state of the material after P-FSSW [61]. Overall, both regions corresponded to the thermo-mechanically stirred area.

Since different mechanical properties correspond to varying thermal diffusivities [62–64], it was verified that these distinct structures produced different thermal responses. Consequently, two separate thresholds were defined for a two-level segmentation, aiming to assess the ability of thermography to distinguish between these areas in a non-destructive way. Thus, three levels of segmentation were obtained, values 1 and 2 being applied for the two different morphologies of the welded area and 0 for each pixel, in which the NTC was lower than the first threshold, obtaining the map in Fig. 7 c. The pixels with NTC > 35.7 were assigned a value of 2, those with 35.7 > NTC > 15.5 were assigned a value of 1, and those with NTC < 15.5 were assigned a value of 0. A morphological closing operation was performed to fill small voids and smooth the edges of segmented shapes using the MATLAB *imclose* command (*A_m_f(:,:) = imclose(A_m(:,:), se)*), with a disk-shaped structuring element of radius 1 pixel. To measure the welded area, the number of pixels corresponding to each segmented region was counted: pixels with a value of 1 (first morphology) and those with a value of 2 (second morphology). These pixel counts were then converted into mm^2 using the mm/pixel ratio. This approach provided an accurate quantitative measurement of the total welded area as well as the specific areas associated with each morphological structure.

The same NTC threshold values obtained during the calibration with specimen P1 were applied to verify this capability. The results of the thermographic segmentation were then compared with those from fractographic analysis. The described procedure has been resumed in Fig. 8.

After verifying the calibration of the thermographic technique, segmentation was performed on the NTC images from each test of the second group of specimens designated for destructive tensile-shear testing, as previously described and resumed in Fig. 8. Quantitative measurements of the welded regions were obtained, considering the total welded area (regardless of morphological differences) and the area of each morphology. This analysis aimed to evaluate the influence and effects of the different morphologies on the joint's final mechanical strength.

The second group of specimens was then subjected to tensile-shear tests, as previously described, with a displacement rate of 1 mm/min. The maximum force recorded for each welded joint was considered indicative of the mechanical strength of the inspected P-FSSW

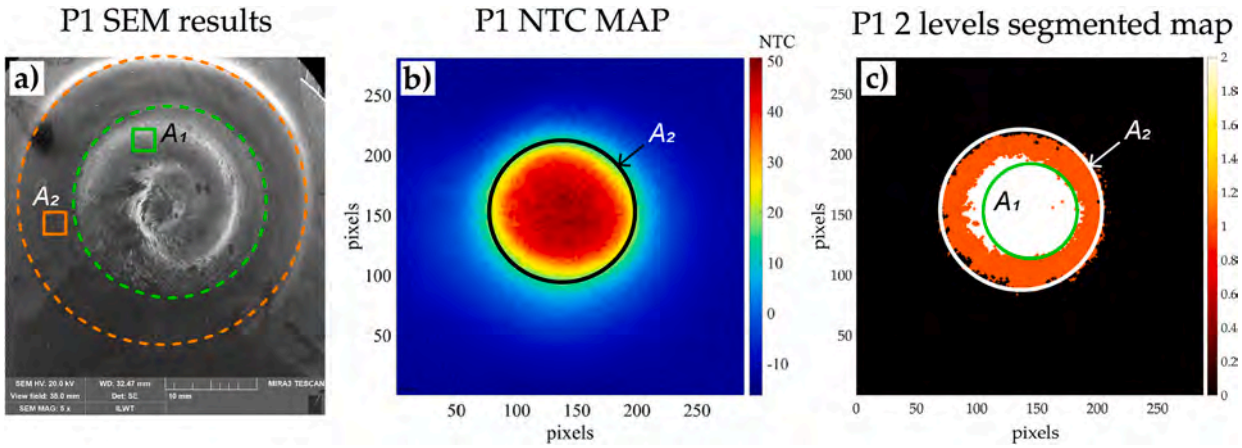

Fig. 7. (a) SEM of the overall fracture surface on the upper sheet of specimen P_1: green circle represents mixed fracture (marked A_1), orange circle indicates the area of ductile behaviour (marked A_2). (b) NTC map obtained for the first cooling frame for specimen P_1: the black circle defines the nominal dimension of spot joint. (c) overlapping between NTC map after segmentation process and SEM results for different morphologies.

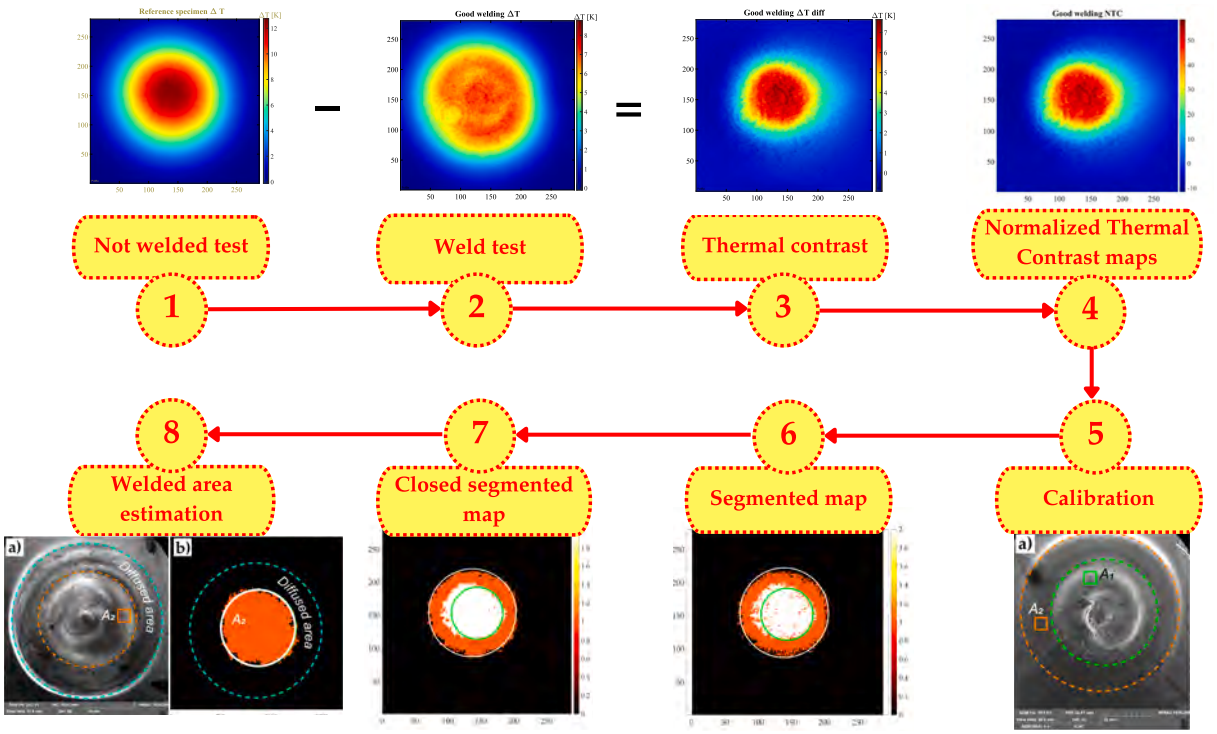

Fig. 8. A schematic resume of thermographic procedure proposed.

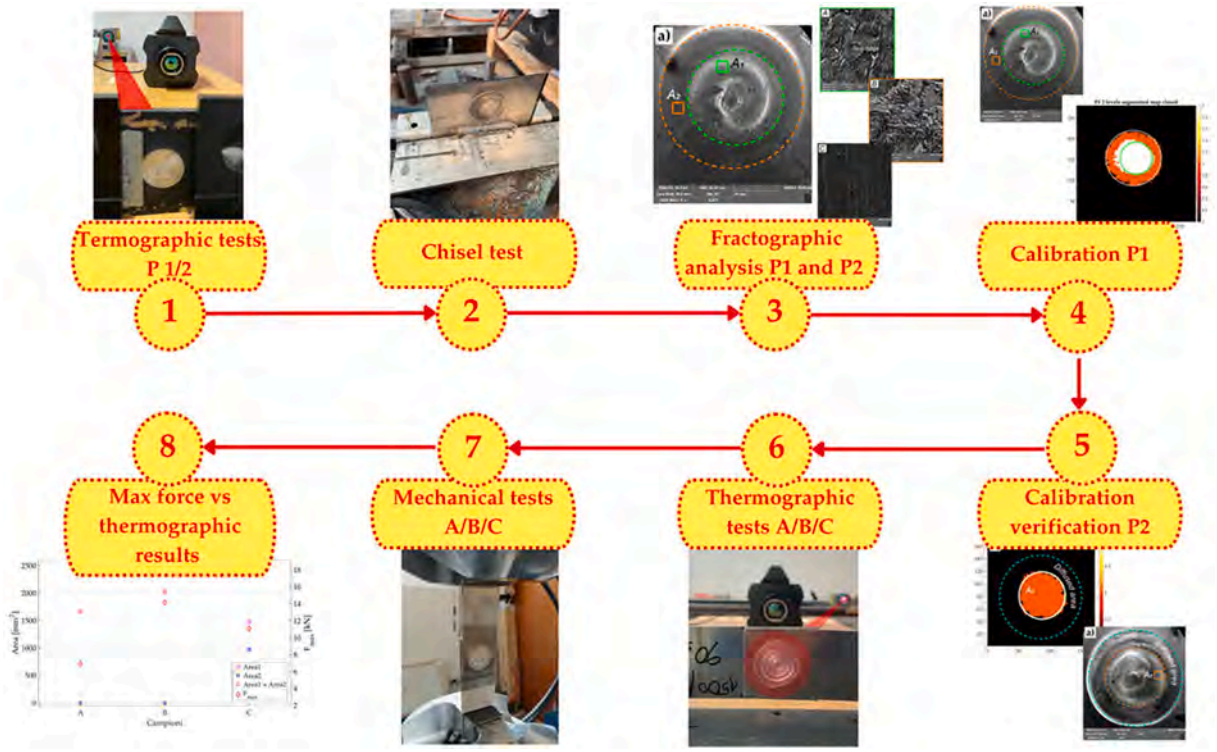

Fig. 9. Scheme of the methods adopted for the experimental phase.

joints.

The results from the thermographic tests—specifically, the quantification of the welded area within the joint—and those from the mechanical tests, indicating the maximum force, were analysed using statistical methods. This analysis aimed to identify the influence of the considered variables on the joint's final mechanical strength. Additionally, it sought to develop a predictive model that could estimate the joint's mechanical strength based on the results obtained through non-destructive thermographic methods. The methodology employed is summarized graphically in Fig. 9.

3. Results and discussion

Considering that two specimens were analysed for calibration, Fig. 11 presents the results obtained in this phase. As detailed in the previous section, based on the SEM results for specimen P1, a dual-threshold segmentation approach was proposed to distinguish between two morphologies. In Fig. 7, two distinct areas can be observed: white and orange. The white area corresponds to the morphology exhibiting mixed failure, while the orange represents the morphology exhibiting ductile failure. The ductile structure corresponds to a lower NTC value, while the mixed structure corresponds to a higher NTC value.

To understand this distinction, it is essential to consider the meaning of a high NTC value. As described in the previous section, the observed thermal contrast reflects the thermal behaviour considered as the difference with respect to the unwelded reference. Due to its higher thermal resistance to heat transfer between the two plates, the unwelded reference (Fig. 5) exhibits a higher surface temperature under the same energy density input compared to the welded case. When welding succeeds, the material continuity reduces the thermal contact resistance, leading to a lower surface temperature than the unwelded case.

Prior research related to the present experimental campaign have demonstrated a direct linear influence of rotational speed on material softening and stirring intensity between plates [23]. It was shown that an increase in rotational speed above 2000 rpm promotes intensive material flow, resulting in the formation of a centreline hook defect. Therefore, considering the thermophysical characteristics of the welded region, accounting for the microstructural variations induced by the thermomechanical welding process, two scenarios can be envisioned. The region may exhibit either a hard and brittle, a "soft" and ductile or mixed behaviour. Given the known inverse correlation between hardness and thermal diffusivity in metallic materials [62–64], in the case of a ductile welded region, higher thermal diffusivity is expected. Conversely, lower thermal diffusivity is expected in a hard and brittle (or mixed) welded region. Considering both as welded area, the structure with lower thermal diffusivity, mixed region, resulting in a higher NTC value than the ductile case.

As illustrated in Fig. 11, applying the thresholds derived from SEM-thermographic comparisons for specimen P1 to specimen P2, a welded region significantly smaller than the nominal tool size was identified, highlighted in orange on Fig. 11a. As depicted in Fig. 10 c-d, the inner region of this specimen contained ductile behaviour. In contrast, the outer region lacked these characteristic features, suggesting a predominant diffusion bonding mechanism (Fig. 10 a). Comparing the thermographic results with SEM data for specimen P2 (Fig. 11 b), it is evident that the proposed calibration thresholds successfully distinguish between the two regions and measure the thermo-mechanically stirred area. The discrepancy between the thermographic and SEM measurements was approximately 6 % (Table 2).

It should be noted that the observed 6 % deviation can be considered independent of the rotational speed and weld morphology, as the thermographic evaluation is based solely on morphological identification through thermal contrast, without direct dependence on process parameters. The main sources of deviation include differences in spatial resolution between thermographic and SEM imaging, the geometric approximations in measuring SEM areas (assuming ideal circular shapes), and the three-dimensional heat diffusion effects that cause minor blurring at the boundaries of different morphologies. These phenomena may slightly affect the precision of area measurements but do not compromise the effectiveness of the proposed NDT procedure.

Fig. 12 presents segmented maps for all analysed specimens using the calibration thresholds. As shown in the first line of Fig. 12, all specimens produced at the lowest rotational speed (1500 rpm) exhibit significantly smaller thermo-mechanically stirred regions than the nominal tool size. Additionally, low repeatability is evident among the three replicates in the same line, with predominantly one

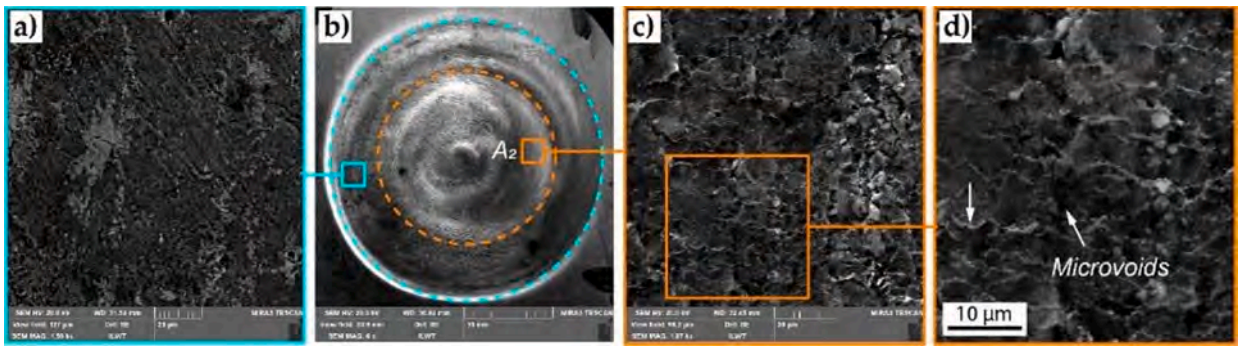

Fig. 10. SEM of specimen P_2: (a) fracture of the outer region (stick condition). (b) overall view of the fracture surface on the upper sheet. (c-d) ductile fracture of the inner region (marked A_2).

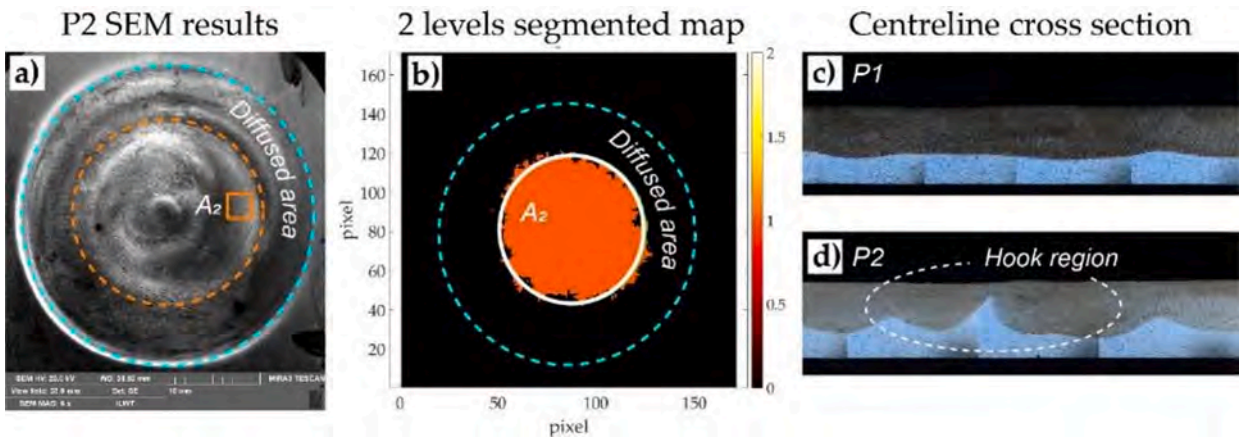

Fig. 11. (A) sem of the overall fracture surface on the upper sheet of specimen p_2: blue circle represents diffused area and orange circle indicates ductile behaviour similar toFig. 7a. b) thermographic results segmented for specimen P_2. (c-d) cross sectional view of the central regions in specimens produced with 2000 rpm (c) and 2500 (d) rotational speeds.

Table 2
Quantitative results obtained for P2 specimen. Difference between thermographic and fractographic measurements of A1 and A2.

Specimen	$A_{1\ SEM}$ (mm^2)	$A_{1\ TT}$ (mm^2)	Difference (%)	$A_{2\ SEM}$ (mm^2)	$A_{2\ TT}$ (mm^2)	Difference (%)
P02	0	0	0	305.7	289.2	5.4

morphology present.

In the second line, corresponding to specimens produced at 2000 rpm, the thermo-mechanically stirred area is larger and generally exhibits a uniform structure, mostly of ductile behaviour. In contrast, specimens C, representing specimens produced at 2500 rpm, shows an increase in the total area with both morphologies. Specimens C exhibit a significant presence of the mixed phase. In Fig. 12, quantitative values for Area 1 (mixed behaviour), Area 2 (ductile fracture), and the total welded area are provided for each specimen.

Compared to conventional NDT methods, the proposed thermographic procedure enables rapid, full-field, contactless detection of morphological defects, including hook formations and incomplete bonding, through local variations in thermal diffusivity. This makes it particularly suited for in-line inspection of P-FSSW joints, where physical contact or volumetric imaging may be less practical.

Fig. 13 also includes a matrix of photographs of the specimens after shear-tensile testing. It is evident that the process exhibits low repeatability for both the first and third columns, as indicated by the thermographic results. This variability is further corroborated by the maximum force results from tensile testing presented in Fig. 14. Specimens produced at 2000 rpm achieved the highest mechanical strength and repeatability, demonstrating that this rotational speed produces the strongest and most consistent joints.

Interestingly, at 2500 rpm, the joint strength decreases, and poor repeatability is evident, as shown by the widely varying maximum force values. Despite the larger thermo-mechanically stirred region for 2500 rpm specimens compared to 2000 rpm, the latter group exhibits superior strength. This discrepancy contrasts with expectations for other spot-welding techniques like RSW or RPW [24–27], where larger fused regions typically correspond to higher strength. This behaviour has been further investigated in a recent study [23], which demonstrated that increasing the rotational speed beyond 2000 rpm leads to excessive plastic flow and the formation of hook-like defects along the centerline. These morphologies act as stress concentrators, ultimately reducing the mechanical strength and repeatability of the joints.

It should also be noted that the heat-affected zone (HAZ) did not show any measurable influence on mechanical strength or thermographic contrast. The microstructural changes induced in the HAZ were minor and insufficient to generate detectable differences in thermal diffusivity, confirming that the weld quality evaluation could be effectively confined to the thermo-mechanically stirred region and adjacent TMAZ.

An example of this behaviour is specimen A_03, which, despite its larger fused area compared to the other two specimens, exhibits reduced F_{max}. This can be attributed to the geometry of the welded region. Unlike the circular and solid welded regions in other specimens, A_03 has ring-shaped weld with an irregular, unwelded central region. This central discontinuity acts as a defect during tensile testing, causing stress concentration that reduces the joint's mechanical strength.

A statistical analysis was performed to evaluate the influence of the different morphologies and total thermo-mechanically stirred area on the final mechanical strength (F_{max}). Several variables were defined, including A_1, A_2, A_{tot}, and the ratios A_1/A_{tot} and A_2/A_{tot}. Correlation analysis was conducted to quantify their relationships with F_{max}. The results, shown in Fig. 15, indicate that A_2 has the strongest correlation with F_{max} ($r = 0.81$), suggesting that this variable is the primary predictor of joint strength. Conversely, A_1 and the A_1/A_{tot} ratio exhibit weak negative correlations, indicating that higher values of these variables tend to reduce the joint's mechanical strength.

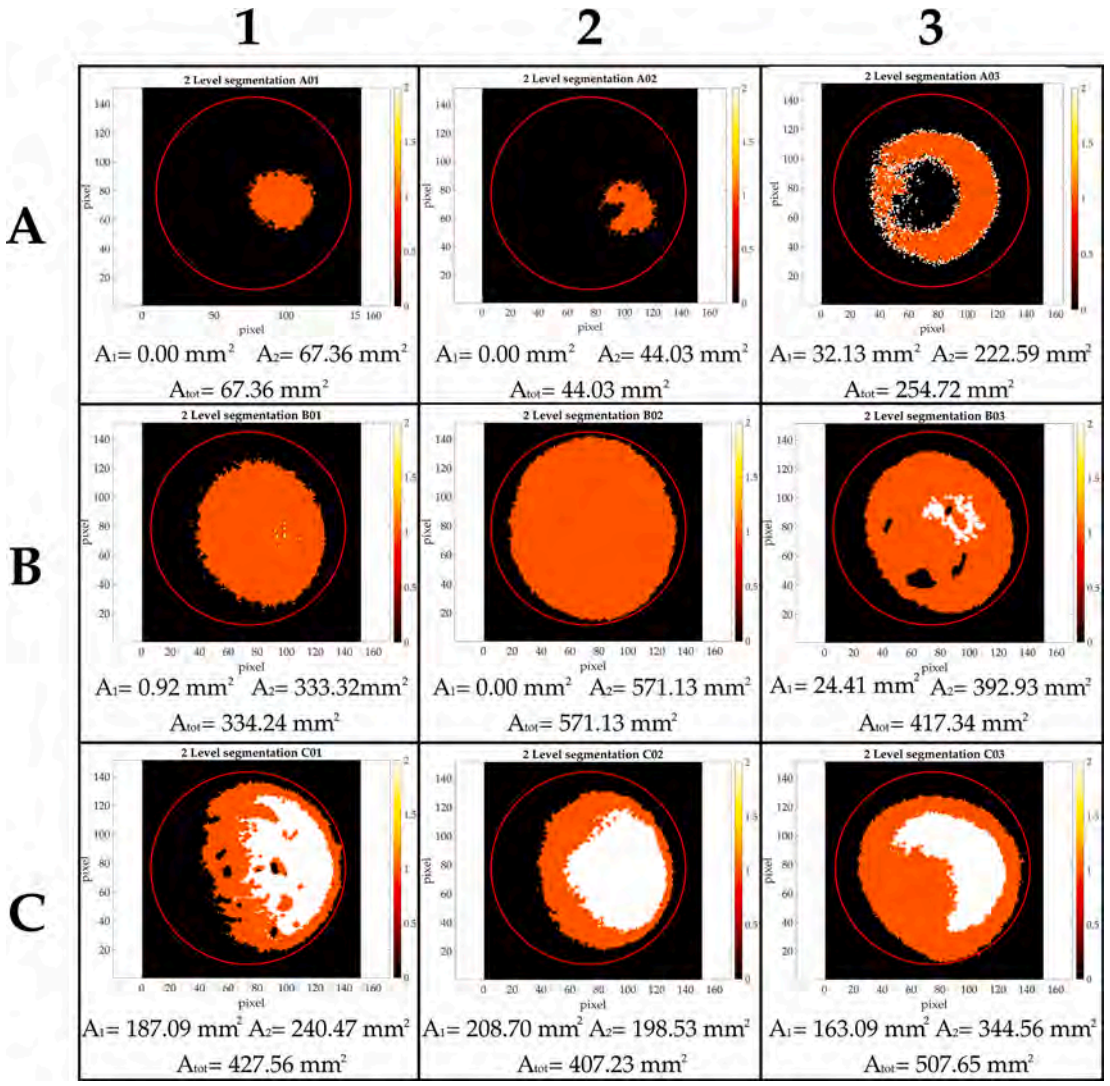

Fig. 12. Thermographic results for specimens undergoing tensile-shear test. The red circle indicates the nominal value of welded joint (tool diameter), the orange area depicts the ductile region, and the white area corresponds to the mixed behaviour.

A linear regression model was developed to incorporate these variables. The model with the highest adjusted R^2(0.603) included an interaction term between A_1 and A_2 ($A_1 \bullet A_2$), labelled "*Interaction*" in Fig. 15 B. However, the statistical significance of the interaction term was limited, with a p-value of ~ 0.05. Including rotational speed as a variable in the model did not improve its statistical significance.

These findings suggest that while A_2 is the most significant individual predictor of joint strength, the interaction effects between morphologies and geometric factors warrant further investigation to refine predictive models.

The regression model with interaction obtained is as follows:

$$F_{max} = 7.139 - 0.054 \bullet A_1 + 0.013 \bullet A_2 + 0.0003 \bullet A_1 A_2$$

However, considering the significance of each coefficient, specifically the p-value summarized in the Table 3, it can be observed that the coefficients related to A1 are not significant. Thus, although the full model with interaction explains the variability of F_{max} slightly better than the simplified model with only A_2—with an adjusted R^2 of 0.603 compared to 0.598 for the simplified model—the global p-value of the simplified model is 0.0088, making it statistically significant. In contrast, the p-value for the interaction model is approximately 0.05. Despite the low statistical significance, A1 may still influence strength due to local inhomogeneities or weak bonding, acting as possible crack initiation sites.

Moreover, evaluating the F-statistic, which compares the current model to a constant model, the simplified model achieves a value of 12.9, compared to 5.06 for the interaction model. This indicates that the interaction model is similar to the constant model, which uses only the mean of F_{max} as the prediction.

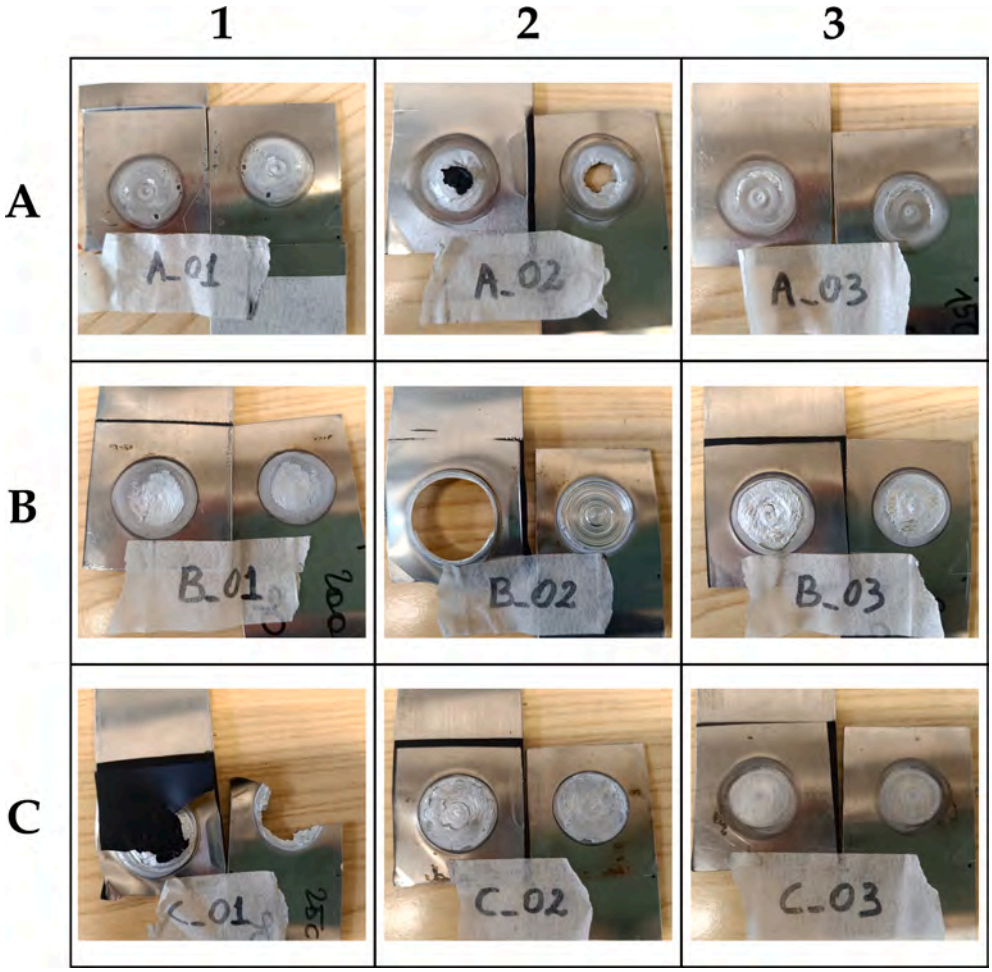

Fig. 13. Pictures after tensile-shear mechanical tests for each test for specimens A-B-C 1/2/3.

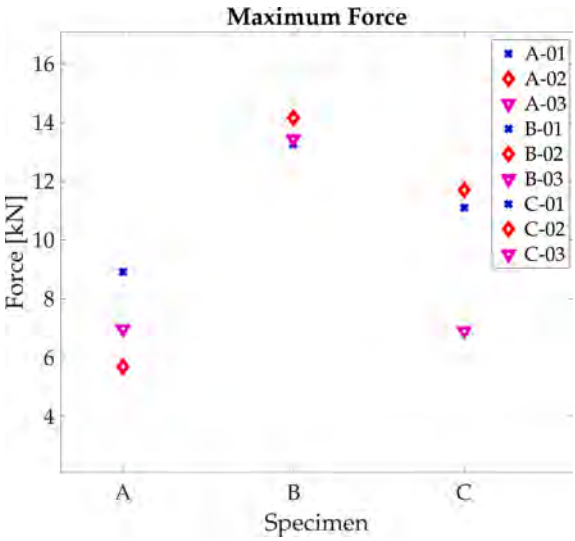

Fig. 14. Values of F_{max} of specimens tested.

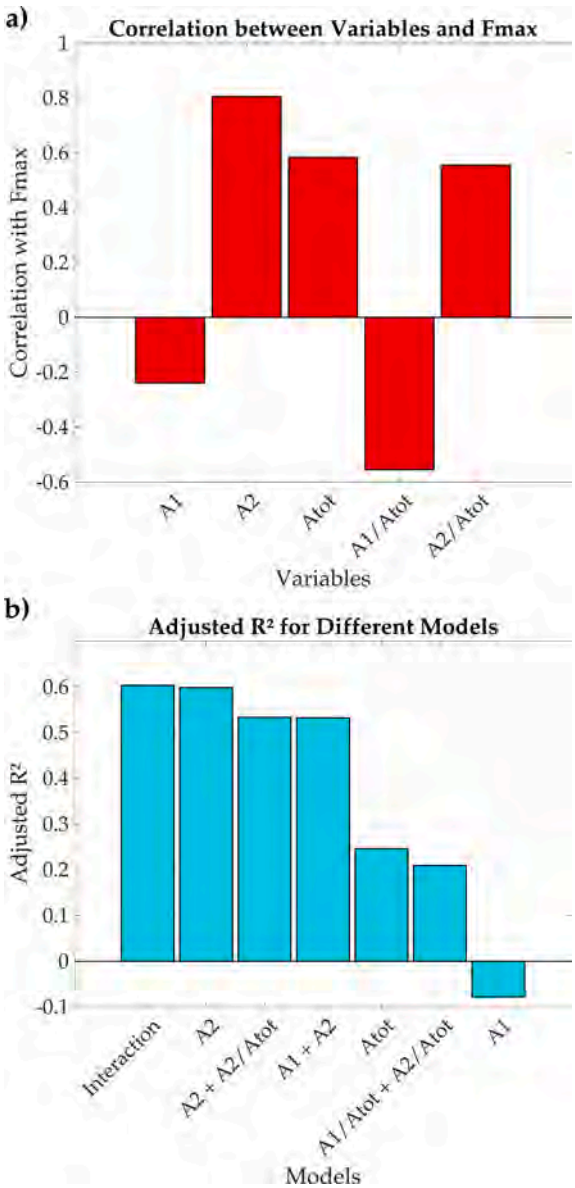

Fig. 15. A) histogram of correlations coefficient among parameters investigated and fmax. b) histogram of adjusted r2 values for each model.

Table 3
Results of statistical analyses for the proposed models.

Coefficient	Value estimation	Standard error	t-stat	p-value	Significant?
β_0 **(intercept)**	7.1385	1.5022	4.752	0.0051	Yes ($p < 0.05$)
β_1 **(A_1)**	−0.0540	0.0376	−1.4385	0.2098	No ($p > 0.05$)
β_2 **(A_2)**	0.0125	0.0047	2.6694	0.0444	Yes ($p < 0.05$)
β_3 **(A_1 A_2)**	0.0003	0.0002	1.4448	0.2081	No ($p > 0.05$)

Therefore, the simplified model with only A2 is preferred, as shown below:

$$F_{max} = 6.641 + 0.015 \bullet A_2$$

4. Conclusions

This study proposes a fully non-destructive procedure for evaluating the mechanical strength of dissimilar aluminium welded joints

produced through novel probeless friction stir spot welding (P-FSSW) technique. The proposed procedure, based on step laser thermography technique, enables quantitative analysis of the thermo-mechanically stirred region in P-FSSW joints, with the ability to distinguish between two types of structures present in the welded region.

A thermographic procedure was developed using extended heating via a circular laser spot with a Gaussian energy distribution.

Eleven spot joints were analysed to assess the influence of the thermo-mechanically stirred area. The first two specimens were obtained using different rotational speeds (1500 rpm and 2500 rpm) and were subjected to thermographic testing, Chisel tests, and fractographic analysis. The remaining nine joints, produced with three rotational speeds (1500 rpm, 2000 rpm, and 2500 rpm), were tested by thermographic method and then subjected to tensile-shear tests to evaluate their mechanical strength.

The first two specimens were used to calibrate the proposed thermographic procedure, which addresses the issue of non-uniform energy distribution within the laser spot using reference specimens. The signals from these references were subtracted from the sequences obtained during tests on the produced joints. The calibrated procedure was validated through Chisel tests and fractographic analysis using SEM, which revealed the presence of two distinct morphologies in the welded area within the thermo-mechanically stirred region: a mixed structure and a ductile one (A_1 and A_2). The technique was calibrated by analysing the thermographic map of one of the two specimens, defining thresholds to distinguish the two structures identified in the fractographic analysis. This calibration was then verified on the second specimen, yielding a difference of approximately 6 % between the thermographic and SEM measurements.

The same procedure was applied to the joints subsequently subjected to tensile-shear tests to evaluate the correlation between the welded area and mechanical strength, focusing on F_{max}. All thermographic maps were analysed to measure the area of each structure and the total welded area. Statistical analyses were then conducted to verify the correlation between A_1, A_2, and F_{max}, revealing that A_2 had the strongest correlation with F_{max} ($r = 0.81$). Other parameters, such as A_{tot}, A_1/A_{tot}, and A_2/A_{tot}, were also considered but showed weaker correlations.

Once the most significant parameters were identified, an empirical regression model for F_{max} as a function of A_1 and A_2 was proposed. The model that initially best described Fmax (adjusted $R^2 = 0.603$) included an interaction term $A_1{*}A_2$; however, the statistical significance of this interaction was moderate, with a p-value close to 0.05. Further examination of the model's coefficients revealed that those associated with A_1 were insignificant. Consequently, a simplified model considering only A_2 was preferred, as it achieved a comparable adjusted R^2 of 0.598 while demonstrating higher statistical reliability with a global p-value of 0.0088.

The results suggest that the step laser thermography methodology, coupled with the proposed analysis, provides a reliable and non-destructive approach for evaluating the mechanical properties of P-FSSW joints. However, further refinement of the model and investigation of additional influencing factors may enhance the predictive capability of this methodology. Compared to conventional pulsed thermography, the proposed long-pulsed laser approach offers several advantages for industrial non-destructive quality control. These include the possibility of using low-cost and low-power laser sources, a reduced need for precise control over the heating pulse, and improved robustness against thermal reflections and material inhomogeneities. These features make the method particularly suitable for full-field, in-line inspections of P-FSSW joints in industrial environments.

To further improve and extend the applicability of the proposed methodology, the following next steps are identified:

- Increasing the laser pulse duration to allow low-power and low-cost lasers, thereby reducing equipment costs and operator risks while eliminating the need for surface coatings.
- Developing and adapt advanced post-processing algorithms tailored to the increased pulse duration to optimize the analysis and enhance accuracy.
- Designing and implement a prototype system based on the developed procedure for in-situ analysis of this type of weld, enabling real-time quality assessment in industrial applications.

Future developments will specifically explore the use of lower-power laser sources (e.g., <10 W) combined with longer heating durations, maintaining constant energy input to ensure sufficient thermal excitation while significantly reducing equipment cost and operational risk.

Funding:

This research is funded by the European Union – NextGenerationEU (National Sustainable Mobility Center CN00000023, Italian Ministry of University and Research Decree n. 1033 – 17/06/2022, Spoke 11 (Innovative Materials and Lightweighting), and partly supported by the "World-Class Science Center" program Advanced Digital Technologies (Grant Agreement No. 075–15-2022–312, dated 20 April 2022).

CRediT authorship contribution statement

G. Dell'Avvocato: Writing – original draft, Visualization, Validation, Methodology, Investigation, Formal analysis, Data curation, Conceptualization. **M. Rashkovets:** Writing – review & editing, Visualization, Investigation, Formal analysis, Data curation, Conceptualization. **E. Mancini:** Writing – review & editing, Supervision, Resources. **N. Contuzzi:** Writing – review & editing, Validation, Supervision, Resources, Formal analysis. **G. Casalino:** Writing – review & editing, Supervision, Resources, Funding acquisition. **D. Palumbo:** Writing – review & editing, Supervision, Formal analysis, Data curation. **U. Galietti:** Supervision, Resources, Project administration, Funding acquisition.

Declaration of competing interest

The authors declare that they have no known competing financial interests or personal relationships that could have appeared to influence the work reported in this paper.

Data availability

Data will be made available on request.

References

[1] Z. Csereklyei, D.I. Stern, Flying more efficiently: joint impacts of fuel prices, capital costs and fleet size on airline fleet fuel economy, Ecol. Econ. 175 (2020), https://doi.org/10.1016/j.ecolecon.2020.106714.

[2] K. Dahal, S. Brynolf, C. Xisto, J. Hansson, M. Grahn, T. Grönstedt, M. Lehtveer, Techno-economic review of alternative fuels and propulsion systems for the aviation sector, Renew. Sustain. Energy Rev. 151 (2021), https://doi.org/10.1016/j.rser.2021.111564.

[3] Z. Wang, B. Dong, Y. Wang, M. Li, H. Liu, F. Han, Analysis and evaluation of fuel cell technologies for sustainable ship power: Energy efficiency and environmental impact, Energy Convers. Manage.: X 21 (2024), https://doi.org/10.1016/j.ecmx.2023.100482.

[4] A.G. Olabi, T. Wilberforce, M.A. Abdelkareem, Fuel cell application in the automotive industry and future perspective, Energy 214 (2021), https://doi.org/10.1016/j.energy.2020.118955.

[5] Y. Gao, Z. Li, X. Wei, Z. Zhou, J. Xiong, Y. Du, Y. Du, Advanced lightweight composite shells: manufacturing, mechanical characterizations and applications, Thin-Walled Struct. 204 (2024), https://doi.org/10.1016/j.tws.2024.112286.

[6] W. Zhang, J. Xu, Advanced lightweight materials for Automobiles: A review, Mater Des 221 (2022), https://doi.org/10.1016/j.matdes.2022.110994.

[7] S. Rohani Nejad, S. Hesari, S.M.H. Mirbagheri, Effect of nickel and copper shells on mechanical properties of advanced lightweight TPU metamaterials during uniaxial compression, Sci Rep 14 (2024), https://doi.org/10.1038/s41598-024-82317-7.

[8] M. Ivanov, A. Cherniavsky, A. Tingaev, Y. Bezgans, D. Derbenev, N. Shaburova, I. Suleymanova, A. Alrukhaymi, T. Sonar, Experimental and numerical investigation on cold cracking susceptibility of naval grade high strength steel welds for lightweight shipbuilding structures, International Journal of Lightweight Materials and Manufacture 7 (2024) 597–613, https://doi.org/10.1016/j.ijlmm.2024.03.004.

[9] A. Cusanno, D. Carty, G. Palumbo, A novel methodology for affecting the strain paths during hydraulic bulge tests by means of laser heat treatments, European Journal of Mechanics, A/solids 111 (2025), https://doi.org/10.1016/j.euromechsol.2025.105569.

[10] S. Al-Alimi, N.K. Yusuf, A.M. Ghaleb, M.A. Lajis, S. Shamsudin, W. Zhou, Y.M. Altharan, H.S. Abdulwahab, Y. Saif, D.H. Didane, I. S T T, A. Adam, Recycling aluminium for sustainable development: A review of different processing technologies in green manufacturing, Results in Engineering 23 (2024). doi: 10.1016/j.rineng.2024.102566.

[11] S.J. Doshi, A. V Gohil, N.D. Mehta, R. Vaghasiya, Challenges in Fusion Welding of Al alloy for Body in White, 2018. www.sciencedirect.comwww.materialstoday.com/proceedings.

[12] M. Kimura, Y. Sano, M. Kusaka, K. Kaizu, Methods for improving joint strength of friction stud welded AA5083 alloy joints, Journal of Advanced Joining Processes 5 (2022), https://doi.org/10.1016/j.jajp.2021.100075.

[13] J. Zhang, Q. Liu, Y. Huang, Influence of heat input on pinless friction stir spot welding of aluminum–copper dissimilar materials, Mater Charact 218 (2024), https://doi.org/10.1016/j.matchar.2024.114456.

[14] M. Thomä, A. Gester, G. Wagner, B. Straß, B. Wolter, S. Benfer, D.K. Gowda, W. Fürbeth, Application of the hybrid process ultrasound enhanced friction stir welding on dissimilar aluminum/dual-phase steel and aluminum/magnesium joints, Materwiss Werksttech 50 (2019) 893–912, https://doi.org/10.1002/mawe.201900028.

[15] C. Meengam, Y. Dunyakul, D. Maunkhaw, Joint dissimilar diffusion bonding of SSM-ADC12 Al alloy to SSM 6063 Al alloy, Mater Today Proc (2023), https://doi.org/10.1016/j.matpr.2023.05.392.

[16] H. Li, C. Zhang, Y. Deng, K. Zhou, Z. Ni, F. Yan, Q. Liu, Interfacial reactions and joint performances of high-power ultrasonic welding of aluminum to steel, J. Mater. Res. Technol. 26 (2023) 328–343, https://doi.org/10.1016/j.jmrt.2023.07.188.

[17] N. Contuzzi, M. Rashkovets, G. Casalino, Numerical and experimental investigation of probeless friction stir spot welding of a multilayer aluminium alloy compound, Sci. Technol. Weld. Join. 28 (2023) 653–661, https://doi.org/10.1080/13621718.2023.2193460.

[18] A. Reilly, H. Shercliff, Y. Chen, P. Prangnell, Modelling and visualisation of material flow in friction stir spot welding, J Mater Process Technol 225 (2015) 473–484, https://doi.org/10.1016/j.jmatprotec.2015.06.021.

[19] T. Matsuda, K. Owada, A. Numata, H. Shoji, T. Sano, M. Ohata, A. Hirose, Influence of interfacial structure on the fracture behavior of friction stir spot welded dissimilar joints, Mater. Sci. Eng. A 772 (2020), https://doi.org/10.1016/j.msea.2019.138743.

[20] S. Bharti, S. Kumar, I. Singh, D. Kumar, S.S. Bhurat, M.R. Abdullah, S.S. Rahimian Koloor, A Review of Recent Developments in Friction Stir Welding for Various Industrial Applications, J Mar Sci Eng 12 (2024), https://doi.org/10.3390/jmse12010071.

[21] M.M.Z. Ahmed, M.M. El-Sayed Seleman, D. Fydrych, G. Çam, Friction Stir Welding of Aluminum in the Aerospace Industry, The Current Progress and State-of-the-Art Review, Materials 16 (2023), https://doi.org/10.3390/ma16082971.

[22] Y. Zou, W. Li, Z. Shen, Y. Su, X. Yang, Refill friction stir spot welding of aluminum alloys: State-of-the-art and Perspectives, Weld. World 67 (2023) 1853–1885, https://doi.org/10.1007/s40194-023-01552-0.

[23] M. Rashkovets, G. Dell'Avvocato, N. Contuzzi, D. Palumbo, U. Galietti, G. Casalino, On the role of rotational speed in P-FSSW dissimilar aluminum alloys lap weld, Weld. World (2025), https://doi.org/10.1007/s40194-025-02010-9.

[24] D. Palumbo, E. D'Accardi, U. Galietti, A new thermographic procedure for the non-destructive evaluation of RSW joints, in, SPIE-Intl Soc Optical Eng (2019) 23, https://doi.org/10.1117/12.2518979.

[25] G. Dell'Avvocato, D. Palumbo, Thermographic procedure for the assessment of Resistance Projection Welds (RPW): Investigating parameters and mechanical performances, Journal of Advanced Joining Processes 9 (2024), https://doi.org/10.1016/j.jajp.2023.100177.

[26] E.T. Hall, D.I. Crecraft, Bonded joints and non-destructive testing NDT of resistance spots, roll-spot, stitch and seam welds, n.d.

[27] X. Sun, K. Zeng, X. He, L. Zhang, Ultrasonic C-scan imaging and analysis of the mechanical properties of resistance spot-welded joints of stainless steel, Nondestr. Test. Eval. 32 (2017) 242–254, https://doi.org/10.1080/10589759.2016.1241251.

[28] D. Wagner, M. Bernardi, F. Grassel, T. Chen, K. Schimanski, L. Bergmann, B. Klusemann, Analysis of mechanical properties and microstructure of single and double-pass friction stir welded T-joints for aluminium stiffened panels, Mater Des 247 (2024), https://doi.org/10.1016/j.matdes.2024.113438.

[29] R.F. Hamade, A.M.R. Baydoun, Nondestructive detection of defects in friction stir welded lap joints using computed tomography, Mater Des 162 (2019) 10–23, https://doi.org/10.1016/j.matdes.2018.11.034.

[30] S. Krall, M. Prießnitz, C. Baumann, F. Bleicher, Non-destructive characterization of strain induced surface hardness increase by measuring magnetic properties of AISI 304, Mater Des 226 (2023), https://doi.org/10.1016/j.matdes.2023.111627.

[31] C. Summerville, D. Adams, P. Compston, M. Doolan, Nugget Diameter in Resistance Spot Welding: A Comparison between a Dynamic Resistance Based Approach and Ultrasound C-scan, in, Procedia Eng, Elsevier Ltd (2017) 257–263, https://doi.org/10.1016/j.proeng.2017.04.033.

[32] P. Liu, E. Zhao, J. Meng, X. Zhou, C. Liu, H. Tian, J. Li, X. Zhao, J. Zhang, H. Zhao, C. Qi, On-line measurement of nugget diameter in automatic resistance spot welding based on embedded ultrasound probe, Measurement (lond) 226 (2024), https://doi.org/10.1016/j.measurement.2023.114095.

[33] V. Vijayan, J. Changwook, Y. Do Park, An Investigation into the Measurement and Evaluation of Volumetric Voids in Advanced High Strength Steel Resistance Spot Welds, J Mater Eng Perform (2024), https://doi.org/10.1007/s11665-024-10241-y.
[34] E. Ghafarallahi, G.H. Farrahi, N. Amiri, Acoustic simulation of ultrasonic testing and neural network used for diameter prediction of three-sheet spot welded joints, J Manuf Process 64 (2021) 1507–1516, https://doi.org/10.1016/j.jmapro.2021.03.012.
[35] A.M. Chertov, R.G. Maev, F.M. Severin, Acoustic microscopy of internal structure of resistance spot welds, IEEE Trans Ultrason Ferroelectr Freq Control 54 (2007) 1521–1529, https://doi.org/10.1109/TUFFC.2007.422.
[36] J. Lecompagnon, P.D. Hirsch, C. Rupprecht, M. Ziegler, Nondestructive thermographic detection of internal defects using pixel-pattern based laser excitation and photothermal super resolution reconstruction, Sci Rep 13 (2023), https://doi.org/10.1038/s41598-023-30494-2.
[37] E. D'Accardi, R. Krankenhagen, A. Ulbricht, M. Pelkner, R. Pohl, D. Palumbo, U. Galietti, Capability to detect and localize typical defects of laser powder bed fusion (L-PBF) process: an experimental investigation with different non-destructive techniques, Prog. Addit. Manuf. 7 (2022) 1239–1256, https://doi.org/10.1007/s40964-022-00297-4.
[38] B. Oswald-Tranta, Detection and characterisation of short fatigue cracks by inductive thermography, Quant Infrared Thermogr J (2021), https://doi.org/10.1080/17686733.2021.1953226.
[39] D. Palumbo, R. De Finis, P.G. Demelio, U. Galietti, A new rapid thermographic method to assess the fatigue limit in GFRP composites, Compos B Eng 103 (2016) 60–67, https://doi.org/10.1016/j.compositesb.2016.08.007.
[40] C. Colombo, L. Vergani, Thermographic applications for the rapid estimation of fatigue limit, in: Procedia Structural Integrity, Elsevier B.V., 2019: pp. 658–666. doi: 10.1016/j.prostr.2020.02.058.
[41] W.J. Parker, R.J. Jenkins, C.P. Butler, G.L. Abbott, Flash method of determining thermal diffusivity, heat capacity, and thermal conductivity, J Appl Phys 32 (1961) 1679–1684, https://doi.org/10.1063/1.1728417.
[42] M. Gresil, Z. Wang, Q.A. Poutrel, C. Soutis, Thermal Diffusivity Mapping of Graphene Based Polymer Nanocomposites, Sci Rep 7 (2017), https://doi.org/10.1038/s41598-017-05866-0.
[43] J.C. Krapez, L. Spagnolo, M. Frieß, H.P. Maier, G. ünter Neuer, Measurement of in-plane diffusivity in non-homogeneous slabs by applying flash thermography, Int. J. Therm. Sci. 43 (2004) 967–977, https://doi.org/10.1016/j.ijthermalsci.2004.02.003.
[44] L. Gaverina, M. Bensalem, A. Bedoya, J. González, A. Sommier, J.L. Battaglia, A. Salazar, A. Mendioroz, A. Oleaga, J.C. Batsale, C. Pradere, Constant Velocity Flying Spot for the estimation of in-plane thermal diffusivity on anisotropic materials, Int. J. Therm. Sci. 145 (2019), https://doi.org/10.1016/j.ijthermalsci.2019.106000.
[45] M. Colom, A. Bedoya, A. Mendioroz, A. Salazar, Measuring the in-plane thermal diffusivity of moving samples using laser spot lock-in thermography, Int. J. Therm. Sci. 151 (2020), https://doi.org/10.1016/j.ijthermalsci.2020.106277.
[46] P. Bison, F. Cernuschi, S. Capelli, A thermographic technique for the simultaneous estimation of in-plane and in-depth thermal diffusivities of TBCs, Surf Coat Technol 205 (2011) 3128–3133, https://doi.org/10.1016/j.surfcoat.2010.11.013.
[47] T. Sriyubol, U. Nontakaew, T. Chantrasmi, Analysing sizing defects in brazing joints using pulse phase thermography with a cross-correlation maximisation technique, Quant Infrared Thermogr J 13 (2016) 144–154, https://doi.org/10.1080/17686733.2016.1145843.
[48] P. Myrach, F. Jonietz, D. Meinel, H. Suwala, M. Ziegler, Calibration of thermographic spot weld testing with X-ray computed tomography, Quant Infrared Thermogr J 14 (2017) 122–131, https://doi.org/10.1080/17686733.2017.1281554.
[49] L. Santoro, V. Razza, M. De Maddis, Frequency-based analysis of active laser thermography for spot weld quality assessment, Int. J. Adv. Manuf. Technol. 130 (2024) 3017–3029, https://doi.org/10.1007/s00170-023-12845-5.
[50] L. Santoro, V. Razza, M. De Maddis, Nugget and corona bond size measurement through active thermography and transfer learning model, Int. J. Adv. Manuf. Technol. 133 (2024) 5883–5896, https://doi.org/10.1007/s00170-024-14096-4.
[51] D. Palumbo, U. Galietti, Characterisation of steel welded joints by infrared thermographic methods, Quant Infrared Thermogr J 11 (2014) 29–42, https://doi.org/10.1080/17686733.2013.874220.
[52] G. Dell'Avvocato, D. Gohlke, D. Palumbo, R. Krankenhagen, U. Galietti, Quantitative evaluation of the welded area in Resistance Projection Welded (RPW) thin joints by pulsed laser thermography, in: N.P. Avdelidis, A. Mendioroz (Eds.), Thermosense: Thermal Infrared Applications XLIV, SPIE, 2022, p. 26, https://doi.org/10.1117/12.2618806.
[53] I. Kryukov, M. Hartmann, S. Bohm, M. Mund, K. Dilger, F. Fischer, Defect Detection in Friction Stir Welding by Online Infrared Thermography, Journal of Welding and Joining 32 (2014) 50–57, https://doi.org/10.5781/jwj.2014.32.5.50.
[54] L.M. Serio, D. Palumbo, U. Galietti, L.A.C. De Filippis, A.D. Ludovico, Monitoring of the friction stir welding process by means of thermography, Nondestr.Test. Eval. 31 (2016) 371–383, https://doi.org/10.1080/10589759.2015.1121266.
[55] J.C. Zalawadia, S.N. Soman, Infrared Thermography for Monitoring Friction Stir Welding – A Review, in: AIP Conf Proc, American Institute of Physics Inc., 2023. doi: 10.1063/5.0168190.
[56] G. Dell'Avvocato, M. Rashkovets, A. Castellano, D. Palumbo, N. Contuzzi, G. Casalino, U. Galietti, Preliminary procedure for the assessment of probeless friction stir spot welds (P-FSSW) in dissimilar aluminum alloys by long pulsed laser thermography, in: N.P. Avdelidis, G. Ferrarini, F. López (Eds.), Thermosense: Thermal Infrared Applications XLVI, SPIE, 2024: p. 17. doi: 10.1117/12.3013618.
[57] E. D'Accardi, D. Palumbo, R. Tamborrino, U. Galietti, A quantitative comparison among different algorithms for defects detection on aluminum with the pulsed thermography technique, Metals (basel) 8 (2018), https://doi.org/10.3390/met8100859.
[58] F. Jonietz, P. Myrach, H. Suwala, M. Ziegler, Examination of Spot Welded Joints with Active Thermography, J Nondestr Eval 35 (2016) 1–14, https://doi.org/10.1007/s10921-015-0318-4.
[59] L. Kastner, S. Ahmadi, F. Jonietz, P. Jung, G. Caire, M. Ziegler, J. Lambrecht, Classification of Spot-Welded Joints in Laser Thermography Data Using Convolutional Neural Networks, IEEE Access 9 (2021) 48303–48312, https://doi.org/10.1109/ACCESS.2021.3063672.
[60] V. Vavilov, Evaluating the efficiency of data processing algorithms in transient thermal NDT, Thermosense XXVI (2004), https://doi.org/10.1117/12.537604.
[61] T. Kobayashi, Strength and fracture of aluminum alloys, 2000. www.elsevier.com/locate/msea.
[62] J.-C. Krapez, R.L. Voti, Effusivity depth profiling from pulsed radiometry data: comparison of different reconstruction algorithms, n.d.
[63] H. Qu, C. Wang, X. Guo, A. Mandelis, Reconstruction of depth profiles of thermal conductivity of case hardened steels using a three-dimensional photothermal technique, J Appl Phys 104 (2008), https://doi.org/10.1063/1.3035831.
[64] G. Dell'Avvocato, P. Bison, M.E. Palmieri, G. Ferrarini, D. Palumbo, L. Tricarico, U. Galietti, Non-destructive estimation of mechanical properties in Usibor® 1500 via thermal diffusivity measurements: A thermographic procedure, NDT and E Int. 143 (2024), https://doi.org/10.1016/j.ndteint.2023.103034.